DISCRETE AND CONTINUOUS
DYNAMICAL SYSTEMS SERIES B
Volume **19**, Number **1**, January **2014**

doi:10.3934/dcdsb.2014.19.257

pp. **257–279**

A DYNAMICS APPROACH TO A LOW-ORDER CLIMATE MODEL

James Walsh

Department of Mathematics
Oberlin College
10 N. Professor St
Oberlin, OH 44074, USA

Esther Widiasih

Department of Mathematics
University of Hawai'i West Oahu
91-1001 Farrington Hwy
Kapolei, HI, 96707, USA

(Communicated by Miguel Sanjuan)

Abstract. Energy Balance Models (EBM) are conceptual models which have proved useful in the study of planetary climate. The focus of EBM is placed on large scale climate components such as incoming solar radiation, albedo, outgoing longwave radiation and heat transport, and their interactions. Until recently, their study has centered on equilibrium solutions of an associated model equation, with no consideration of the dynamical nature of these solutions. In this paper we continue and expand upon recent efforts aimed at placing EBM in a more mathematical, dynamical systems context. In particular, the dynamical behavior of several variants of the Budyko-Sellers model, all but one of which involve the movement of glaciers, is shown to reduce to the study of the system on an attracting one-dimensional invariant manifold in an appropriately defined state space.

1. **Introduction.** Mathematical models of planetary climate run the gamut from low-order models, through intermediate complexity models, and up to highly sophisticated planetary system models [11]. Low-order models, the analysis of which can be amenable to dynamical systems techniques, are often formulated via finite-dimensional approximations to systems of PDEs derived from the associated physics (see, for example, [37]). One notable example is provided in [21], where E. Lorenz used a Galerkin projection of an infinite-dimensional model to obtain a system of three ODEs describing long-term atmospheric circulation. Several authors have subsequently studied and made use of Lorenz's model; a bifurcation analysis, for example, was provided in [36], while Lorenz's equations were derived from midlatitude atmospheric flow equations and found to exhibit period-doubling cascades, the Ruelle-Takens scenario, and intermittency in [40]. Dynamical behavior such as Hopf-saddle-node bifurcations of fixed points, quasi-periodic Hopf bifurcations of invariant circles, and chaotic dynamics and strange attractors is found when this system is seasonally (periodically) forced [5].

2010 *Mathematics Subject Classification.* Primary: 35Q86; Secondary: 37N10, 86A40.
Key words and phrases. Climate modeling, invariant manifolds, ice line, bifurcations.

Interestingly, the Lorenz system, which Lorenz described as the "simplest possible atmospheric general circulation model," appears as a special case in a three-dimensional ocean circulation model which is thermally and wind-driven [22]. The Lorenz system was coupled to a three-box model of the North Atlantic to study climate variability in [32], yielding an atmosphere-ocean model comprised of nine ODEs. This coupled model was used to investigate the ways in which subtle nonlinear interactions of the system components affect the climate.

In another low-order atmosphere-ocean model, Galerkin truncations of the fluid dynamical equations are used to arrive at a system of seven ODEs in [39]. Geometric singular perturbation theory and bifurcation analysis are used to study model dynamics, which includes intermittent behavior between periodic and chaotic regimes in parameter space.

Galerkin projections from a system of five PDEs, modeling thermally driven ocean flows, onto a 27-dimensional space are used in [7] to study the Atlantic Multidecadal Oscillation (AMO). The model exhibits rich dynamics as parameters are varied, including period-doubling bifurcations, Hénon-like strange attractors and, when the system is periodically forced, invariant tori. In particular, a periodic attractor with the spatio-temporal signature of the AMO appears via a supercritical Hopf bifurcation as damping of sea surface temperature anomalies is increased.

W. Langford and G. Lewis provide a simple model of spherical convection with which to investigate the observed polar expansion of the Hadley cells in [18]. In this work the Navier-Stokes Boussenesq PDE is numerically solved, yielding a hysteresis bifurcation as the equator-to-pole temperature gradient is varied. The overview [6] contains a wealth of additional references concerning the efficacy of dynamical systems techniques in the study of low-order climate models.

Low-order models such as those mentioned above are often used to investigate low-frequency variability in various components of climate systems. As such, the time frame is typically one of months or years. The present work concerns Energy Balance Models (EBM) which, as the name suggests, begin with consideration of energy into the planetary system (from the planet's star) and energy out of the system (via radiation and other processes). Seasonal variations, for example, play no role in the EBM presented here. The model time frame should be thought of as being on the order of hundreds of thousands of years. Indeed, EBM were introduced to study glacial extent as a function of solar luminosity [8], which is known to have increased significantly over the past few billion years [33]. The models to be presented each admit an attracting one-dimensional invariant manifold in state space, placing them within the context of low-order models.

The goal of the EBM analyzed in this article is to determine the planet's long term, latitudinally averaged surface temperature, which in turn will depend upon only the most salient climate features. These features include incoming solar radiation, albedo, outgoing longwave radiation and meridional heat transport. Due to the approximations used in an EBM of the many physical processes involved in a planet's climate, these models are conceptual in nature, providing a broad view of the dependence of temperature on a few essential climate components. We note, nonetheless, that such simple models play an important role in the study of climate as they "will always be needed if one is to have a chance to understand what the complex general circulation models are doing" ([29], p. 619). The focus here is on the behavior of energy balance models when naturally modified to incorporate a dynamical systems perspective.

The seminal model of Budyko [8] and Sellers [35] is introduced in the following section. In addition, we introduce a discrete dynamical systems approach to the framing of the model. In Section 3 we present and interpret Theorem 3.2 concerning the existence of an invariant manifold in phase space when Budyko's model is coupled with a dynamic boundary between open ocean water and sea ice [41]. This coupled model represents a natural step in the continued mathematical development of energy balance climate models. Theorem 3.2 is then used in Section 4 to analyze, and place in a dynamical context, an enhancement of the Jormungand global climate model [1], which was introduced as a possible alternative to the snowball Earth model of the severe glaciations of the Neoproterozoic Era [14]. The main result centers on the existence of an attracting equilibrium solution for which glaciers exist in tropical latitudes without advancing all the way to the equator.

Section 5 introduces two models which incorporate a continental land mass having a simple topology. We present a summary of this work in the concluding section.

2. Budyko's energy balance model.

2.1. The model equation.

M. Budyko and W. Sellers introduced energy balance models independently in 1969 ([8], [35]). Each model focuses on the balance between incoming solar radiation (or *insolation*), outgoing radiation and heat transport in latitudinal zones. The radiation emitted by the Earth is mainly in the infrared spectrum, and hence is referred to as *outgoing longwave radiation* (OLR). Each model incorporates a heat transport term, which in Seller's model includes fluxes of both water vapor and sensible heat carried by atmospheric currents out of a latitude belt, as well as the flux of sensible heat circulated by ocean currents. We focus on Budyko's model, due to the relative simplicity of both its OLR and heat transport components.

The energy balance equation introduced by Budyko is

$$Qs(y)(1-\alpha(y,\eta)) - (A+BT) - C(T-\overline{T}) = 0, \tag{1}$$

with units of Watts per square meter W m^{-2} (equivalently, Joules per second per square meter J $s^{-1}m^{-2}$). The variable y is the sine of the latitude. As the model assumes a symmetry with respect to the equator, y is taken to lie in the interval $[0,1]$, with $y=0$ corresponding to the equator and $y=1$ corresponding to the north pole. We will refer to y as the "latitude," assuming this will cause no confusion on the reader's part.

The function $T=T(y)$ represents the average annual temperature at latitude y. The global annual average insolation is denoted by Q, while $s(y)$ is the distribution of the insolation over latitude, normalized so that

$$\int_0^1 s(y)dy = 1.$$

The function $\alpha=\alpha(y,\eta)$ is the planetary albedo. Snow and ice, for example, reflect more insolation back into space than does open water (or land), so snow and ice have larger albedo values than does open water (or land). The parameter η typically represents the latitude at which open ocean water meets the edge of the sea ice; we refer to this boundary latitude as the *ice line*. Hence, $Qs(y)(1-\alpha(y,\eta))$ represents the absorption of insolation by the surface at latitude y. In the first two models presented in the following, we assume the surface is comprised entirely of water and ice.

The $(A + BT)$- and $C(T - \overline{T})$-terms in (1) account for the loss of energy at latitude y. The OLR is modeled by the linear term $A + BT$ [12], while $C(T - \overline{T})$ is the meridional heat transport term. Here, $\overline{T}$ is the global annual average surface temperature

$$\overline{T} = \int_0^1 T(y)dy.$$

Thus, the meridional heat transport term encompasses the simple idea that warmer (relative to the global average) latitudes lose heat, while colder latitudes gain heat. We note meridional heat transport has also been modeled as a diffusion process; see [28], for example.

As T represents the annual average temperature in Budyko's formulation, we introduce dynamics into the model as follows. Given a temperature profile $T_0(y)$ and an ice line position η, set

$$\frac{R}{K} \cdot \frac{T_{n+1}(y) - T_n(y)}{(n+1) - n} = Qs(y)(1 - \alpha(y, \eta)) - (A + BT_n(y)) - C(T_n(y) - \overline{T}_n) \quad (2)$$

for $n \geq 0$. Here, $T_n = T_n(y)$ is the temperature distribution at year n, R is the heat capacity of the Earth's surface (we use $R = 4 \times 10^8$ J m^{-2}(°C)$^{-1}$ as in [27]), and $K = 3.15 \times 10^7$ s/yr is the number of seconds in one year. Note the units on each side of (2) are Watts per square meter. The temperature change from year n to year $n + 1$ is then set to be $T_{n+1}(y) - T_n(y) = F(T_n(y), \eta)$, where

$$F(T, \eta) = \frac{K}{R}\left(Qs(y)(1 - \alpha(y, \eta)) - (A + BT) - C\left(T - \overline{T}\right)\right). \quad (3)$$

We thus consider a dynamical version of Budyko's model given by

$$T_{n+1}(y) = T_n(y) + F(T_n(y), \eta), \quad (4)$$

for $n \geq 0$ and with $F(T, \eta)$ as in (3). This discrete, yearly approach to Budyko's model also conforms with work of Graves, Lee and North [12], in which it is argued that the annual cycle is the most appropriate time scale at which to model OLR linearly as a function of T.

We note Budyko's model has also been formulated as a partial differential equation; see, for example, [38].

2.2. **Equilibrium solutions.** An equilibrium solution $T^* = T^*(y)$ of (4) satisfies

$$Qs(y)(1 - \alpha(y, \eta)) - (A + BT^*) - C(T^* - \overline{T^*}) = 0. \quad (5)$$

Integrating (5) with respect to y from 0 to 1 yields

$$Q(1 - \overline{\alpha}(\eta)) - (A + B\overline{T^*}) = 0, \quad \text{where } \overline{\alpha}(\eta) = \int_0^1 s(y)\alpha(y, \eta)dy. \quad (6)$$

Solving (6) for $\overline{T^*}$, plugging the result into (5) and solving the resulting equation for T^* yields

$$\begin{aligned} T^* = T^*(y, \eta) &= \frac{1}{B + C}\left(Qs(y)(1 - \alpha(y, \eta)) - A + C\overline{T^*}\right) \\ &= \frac{1}{B + C}\left(Qs(y)(1 - \alpha(y, \eta)) + Q\frac{C}{B}(1 - \overline{\alpha}(\eta)) - A\left(1 + \frac{C}{B}\right)\right). \end{aligned} \quad (7)$$

Note the equilibrium temperature profile depends explicitly on the position of the ice line η.

The insolation distribution function $s(y)$, which can be computed precisely from astronomical considerations [26], is uniformly approximated to within 2% by $s(y) = 1 + s_2 p_2(y)$, where $p_2(y) = \frac{1}{2}(3y^2 - 1)$ is the second Legendre polynomial and $s_2 = -0.482$ [28]. We use this representation of $s(y)$ in all that follows. As in [38], we set the albedo of open water $\alpha_w = 0.32$, and the snow covered ice albedo $\alpha_s = 0.62$.

We consider the albedo function

$$\alpha(y, \eta) = \frac{\alpha_s + \alpha_w}{2} + \frac{\alpha_s - \alpha_w}{2} \cdot \tanh(M(y - \eta)), \tag{8}$$

where M is a parameter controlling the abruptness of the transition from open ocean to snow covered sea ice. Equation (8) is a continuous approximation to a step function having the values α_w for $y < \eta$ and α_s for $y > \eta$ (see Figure 1). We assume throughout that A, B and C are strictly positive, $Q \geq 100$ and $M \geq 1$.

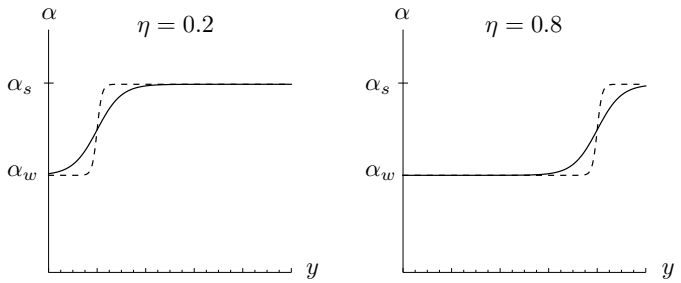

FIGURE 1. The albedo function $\alpha(y, \eta)$ for Budyko's model. Solid line: $M = 10$. Dashed line: $M = 50$.

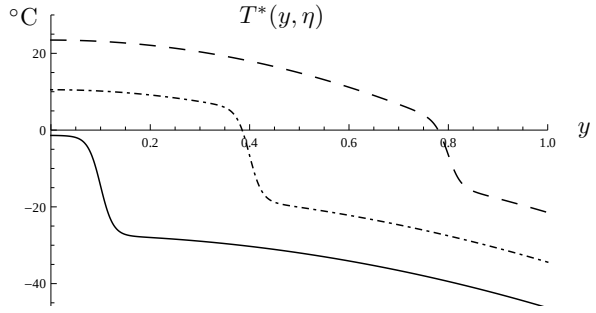

FIGURE 2. Equilibrium solutions of (4). Solid: $\eta = 0.1$. Dash-Dot: $\eta = 0.4$. Dashed: $\eta = 0.8$. Parameters: $Q = 343$, $A = 202$, $B = 1.9$, $C = 3.04$, $M = 40$, $\alpha_w = 0.32$, $\alpha_s = 0.62$.

With these formulations for $s(y)$ and $\alpha(y, \eta)$, we plot various equilibrium solutions $T^*(y, \eta)$ in Figure 2. Once the location of the ice line is specified, the equilibrium temperature profile is completely determined. Alternatively, given any $\eta \in [0, 1]$ there is an equilibrium solution of (4) with the ice line at η.

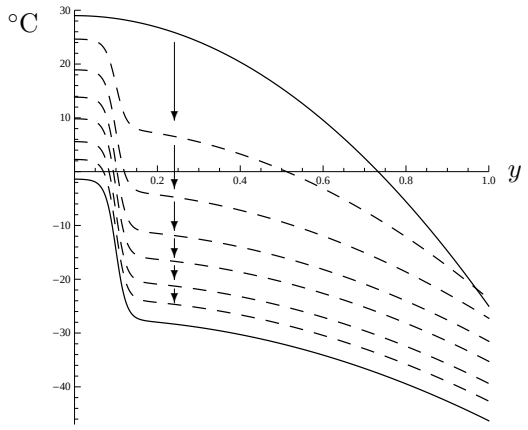

FIGURE 3. The convergence of the initial temperature distribution $T_0(y) = 29 - 54y^2$ to $T^*(y, 0.1)$, evolving under (4). Top graph: T_0. Bottom graph: $T^*(y, 0.1)$. Parameters are as given in Figure 2.

The evolution of the initial temperature profile $T_0(y) = 29 - 54y^2$ under recurrence (4) for $\eta = 0.1$ is presented in Figure 3. This simulation indicates the sequence of temperature profiles converges to $T^*(y, 0.1)$, hinting that the equilibrium solution is stable in an appropriate (and yet to be determined) phase space. A notable deficiency of Budyko's model is also highlighted here: the ice line never moves as the Earth cools down (or heats up, as the case may be) as the sequence $\{T_n\}$ evolves. To enhance the model the ice line will be allowed to vary with temperature, although any such variance will occur slowly relative to changes in the annual average surface temperature. In this setting questions of stability will be addressed.

3. **The coupled Budyko–ice line model.**

3.1. **Further development of Budyko's model.** An equation describing the movement of the ice line, to be coupled with the temperature evolution equation (4), was introduced in [41]. As above, η denotes the latitude of the ice line, $T(y)$ is a temperature profile, and we let T_c denote an annual average critical temperature above which ice melts, and below which ice forms. The ice line displacement is then described by the mapping

$$\eta \mapsto \eta + G(T, \eta) = \eta + \varepsilon(T(\eta) - T_c), \tag{9}$$

where $0 < \varepsilon \ll 1$.

We assume the ice line evolves at a much slower rate than the annual average temperature. Note η increases and the ice line moves toward the north pole if the temperature at the ice line is too high. Similarly, if the ice line temperature is sufficiently low the ice line descends toward the equator.

Given an initial temperature profile $T_0(y)$, an initial ice line latitude η_0 and $n \geq 0$, the coupled temperature and ice line equations are thus given by

$$\begin{aligned} T_{n+1}(y) &= T_n(y) + F(T_n, \eta_n) \\ \eta_{n+1} &= \eta_n + G(T_n, \eta_n), \end{aligned} \tag{10}$$

where $F(T, \eta)$ is given by (3) and $G(T, \eta)$ is as in (9).

3.2. **An invariant manifold theorem.** In this section we outline the proof of a theorem due to Widiasih [41] concerning the dynamics of the coupled temperature–ice line model. First note the ice line $\eta \in [0, 1]$, a manifold with boundary. One approach to incorporating the dynamics at the boundary points $y = 0$ and $y = 1$ is to embed y (and hence η) in $\mathbb{R}$ and appropriately amend (10). For $y \in \mathbb{R}$, set

$$F(T, \eta) = \begin{cases} \frac{K}{R}[Qs(0)(1 - \alpha(y, \eta)) - (A + BT(y)) - C(T(y) - \overline{T})], \text{ when } y < 0 \\ \frac{K}{R}[Qs(y)(1 - \alpha(y, \eta)) - (A + BT(y)) - C(T(y) - \overline{T})], \text{ when } y \in [0, 1] \\ \frac{K}{R}[Qs(1)(1 - \alpha(y, \eta)) - (A + BT(y)) - C(T(y) - \overline{T})], \text{ when } 1 < y, \end{cases} \tag{11}$$

with $\overline{T} = \int_0^1 T(y)dy$. The insolation distribution function is simply set to $s(0)$ for $y < 0$ and to $s(1)$ for $y > 1$, while the albedo function (8) and T are each now defined for $y \in \mathbb{R}$. Embedding y in $\mathbb{R}$ in this way aids in the analysis to follow, in which an inertial manifold is shown to exist. This approach also preserves the dynamics for $y \in (0, 1)$, while allowing for a dynamical analysis of the snowball Earth ($\eta = 0$) and ice free ($\eta = 1$) states.

The mapping of interest becomes

$$\begin{aligned} T_{n+1}(y) &= T_n(y) + F(T_n(y), \eta_n) \\ \eta_{n+1} &= \eta_n + G(T_n(y), \eta_n), \end{aligned} \tag{12}$$

where $F(T, \eta)$ is given by (11) and $G(T, \eta) = \varepsilon(T(\eta) - T_c)$.

Note when $\varepsilon = 0$ the ice line remains fixed and (12) reverts back to (4), albeit with $F(T, \eta)$ as in (11) (compare Figures 2 and 4). In the $\varepsilon = 0$ case the fixed points $(T^*(y, \eta), \eta)$ of (12) take the following form.

Definition 3.1. The *critical set* of (12) is $\mathcal{T}^* = \{(T^*(y, \eta), \eta) : \eta \in \mathbb{R}\}$ where, for a given η,

$$T^*(y, \eta) = \begin{cases} \frac{Q \cdot s(0) \cdot (1 - \alpha(y, \eta)) - A + C \int_0^1 T^*(y, \eta) dy}{B + C}, \text{ when } y < 0 \\ \frac{Q \cdot s(y) \cdot (1 - \alpha(y, \eta)) - A + C \int_0^1 T^*(y, \eta) dy}{B + C}, \text{ when } 0 \leq y \leq 1 \\ \frac{Q \cdot s(1) \cdot (1 - \alpha(y, \eta)) - A + C \int_0^1 T^*(y, \eta) dy}{B + C}, \text{ when } 1 < y. \end{cases} \tag{13}$$

Temperature profiles given by (13) satisfy $F(T^*, \eta) = 0$ (recall equation (7)), where F is given in (11). Several fixed points of (12) in the $\varepsilon = 0$ case are plotted in Figure 4.

The state space for the temperature profiles $T(y)$ is taken to be

$$\mathcal{B} = \{f : \mathbb{R} \to \mathbb{R}, \ f \text{ bounded and continuous}\},$$

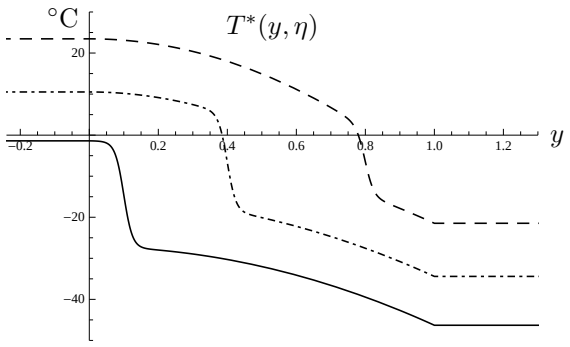

FIGURE 4. Equilibrium solutions of (12) for $\varepsilon = 0$ embedded in $\mathbb{R}$. Solid: $\eta = 0.1$. Dash-Dot: $\eta = 0.4$. Dashed: $\eta = 0.8$. Parameters as in Figure 2.

with $\mathcal{B}$-norm chosen to be the sup norm: $\|f\|_{\mathcal{B}} = \|f\|_\infty$. Define the *dynamic Budyko map*

$$m : \mathcal{B} \times \mathbb{R} \to \mathcal{B} \times \mathbb{R},\ m(T(y),\eta) = (T(y) + F(T(y),\eta),\ \eta + G(T(y),\eta)), \qquad (14)$$

so that iterates of m correspond to recursion (12). Finally, for $(f,x) \in \mathcal{B} \times \mathbb{R}$, set $\|(f,x)\|_{\mathcal{B}\times\mathbb{R}} = \max\{\|f\|_{\mathcal{B}}, |x|\}$.

The estimates used in the proof of Theorem 3.2 below require that constraints be placed on model parameters. In particular, we assume

$$\frac{K(B+C)}{R} < 1, \quad \text{and we set} \quad L = Q \cdot M + A + B + C \qquad (15)$$

in all that follows. By assumption, $L \geq Q \cdot M \geq 100$.

Theorem 3.2. [41] *For sufficiently small ε, there exists an attracting one dimensional invariant manifold for the dynamic Budyko map m. That is,*

1. *There exists a Lipschitz continuous map $\Phi^* : \mathbb{R} \to \mathcal{B}$ such that*
$$\mathcal{P}^* = \{(\Phi^*(\eta), \eta) : \eta \in \mathbb{R}\}$$
is invariant under m.
2. *There exists a closed set $\widetilde{\mathcal{B}} \subset \mathcal{B}$ for which the invariant manifold is attracting. That is, given any $\eta \in \mathbb{R}$, if $T \in \widetilde{\mathcal{B}}$ then the distance between $m^k(T,\eta)$ and $\mathcal{P}^*$ in the $\mathcal{B} \times \mathbb{R}$-norm decreases to 0 exponentially fast, where m^k denotes the k^{th} iterate of m.*

Remark 1. The conclusion of Theorem 3.2 might be viewed as the persistence of an invariant manifold as ε increases from zero. While progress has been made on such persistence problems in the infinite-dimensional context of PDEs and associated semiflows when the unperturbed manifold is normally hyperbolic, less success has been found in applications to inertial manifolds in this setting [3]. The approach taken in [41] for the discrete system (12) is to prove directly the existence of the invariant manifold $\mathcal{P}^*$. As such, this result can be viewed as a contribution to the

study of inertial (smooth, finite dimensional, exponentially attracting invariant) manifolds for perturbations of mappings in Banach spaces.

The proof of Theorem 3.2, which we outline here, is based on Hadamard's graph transform method [30]. Consider the set of graphs

$$\mathcal{G} = \{\Phi : \mathbb{R} \to \mathcal{B},\ \Phi \text{ continuous and uniformly bounded}\}.$$

Let $\Phi \in \mathcal{G}$. We set $\|\Phi\|_{\mathcal{G}} = \sup_{x\in\mathbb{R}} \|\Phi(x)\|_{\mathcal{B}}$,

$$\mathrm{Lip}_{\mathcal{G}}(\Phi) = \sup_{x\neq y} \frac{\|\Phi(x)-\Phi(y)\|_{\mathcal{B}}}{|x-y|}, \quad \text{and} \quad \mathrm{Lip}_{\mathbb{R}}(\Phi(x)) = \sup_{y\neq z} \frac{|\Phi(x)(y)-\Phi(x)(z)|}{|y-z|},$$

the latter for $x \in \mathbb{R}$.

Consider the subset of $\mathcal{G}$ defined by

$$\mathcal{G}_L = \{\Phi \in \mathcal{G} \ :\ \|\Phi\|_{\mathcal{G}} \le L,\ \mathrm{Lip}_{\mathcal{G}}(\Phi) \le L \text{ and } \forall\, x \in \mathbb{R},\ \mathrm{Lip}_{\mathbb{R}}(\Phi(x)) \le L\},$$

with L as in (15). One can show

$$L \ge \max\{\|T^*\|_{\mathcal{G}}, \mathrm{Lip}_{\mathcal{G}}(T^*), \mathrm{Lip}_{\mathbb{R}}(T^*(y,\eta))\},$$

where T^* refers to map

$$T^* : \mathbb{R} \to \mathcal{B}, \quad \eta \mapsto T^*(y,\eta), \tag{16}$$

and $T^*(y,\eta)$ refers to the map $y \mapsto T^*(y,\eta)$ for any given η. In particular, $T^* \in \mathcal{G}_L$.

Lemma 3.3. *If $0 < \varepsilon < 1/(2L)$, then for all $\eta \in \mathbb{R}$, for all $\Phi \in \mathcal{G}_L$, there exists $\beta = \beta(\eta,\Phi) \in \mathbb{R}$ such that $\eta = \beta + G(\Phi(\beta),\beta) = \beta + \varepsilon(\Phi(\beta)(\beta) - T_c)$.*

The number β in Lemma 3.3 is referred to as the "ice line preimage" in [41]. The proof idea is as follows. For $\Phi \in \mathcal{G}_L$, consider

$$H : \mathcal{B} \to \mathcal{B},\ H(f)(x) = \varepsilon(T_c - \Phi(x+f(x))(x+f(x))).$$

Using the defining properties of $\mathcal{G}_L$, one argues that for all $f, g \in \mathcal{B}$, $\|H(f) - H(g)\|_{\mathcal{B}} \le \varepsilon 2L\|f-g\|_{\mathcal{B}}$, so that H is a contraction map on the complete metric space $(\mathcal{B}, \|\cdot\|_{\mathcal{B}})$. Letting $\hat{f} = \hat{f}(\Phi) \in \mathcal{B}$ denote the unique fixed point of H, one has for all $x \in \mathbb{R}$, $\hat{f}(x) = \varepsilon(T_c - \Phi(x+\hat{f}(x))(x+\hat{f}(x)))$. Given $\eta \in \mathbb{R}$, it follows that

$$\eta = \eta + \hat{f}(\eta) + \varepsilon(\Phi(\eta+\hat{f}(\eta))(\eta+\hat{f}(\eta)) - T_c).$$

The preimage is then given by $\beta = \eta + \hat{f}(\eta)$. We note the argument works for any $L > 0$. □

The following estimate is needed in the proof of Theorem 3.2.

Lemma 3.4. *Let $B_0 = 1 - \frac{KB}{R}$, $\delta = \frac{KL}{R}$, and $\kappa = \frac{KB}{R(\delta+B_0L)}$. If*

$$0 < \varepsilon < \min\left\{\frac{1}{4L}, \frac{\kappa}{1+2L\kappa}\right\},$$

then $0 < B_0(1+\rho L) + \rho\delta < 1$, where $\rho = \varepsilon/(1-2\varepsilon L)$.

The proof relies on (15), namely, that $KB/R < K(B+C)/R < 1$ and $L \ge 100 > R/K$. One can show $\varepsilon < 1/(4L)$ implies $0 < \rho < 1$, and that $KB/R < 1$ and $L > R/K$ together imply $0 < \kappa < 1$. One then uses $\varepsilon < \kappa/(1+2L\kappa)$ to get the desired inequality. □

A second application of the Contraction Mapping Theorem yields the function Φ^* in Theorem 3.2.

Lemma 3.5. *Let $\varepsilon > 0$ be as in Lemma 3.4. Let $\Gamma : \mathcal{G}_L \to \mathcal{G}_L$, $\Gamma(\Phi)(\eta) = \Phi(\beta) + F(\Phi(\beta), \beta)$, where $\eta = \beta + \varepsilon(\Phi(\beta)(\beta) - T_c)$ as in Lemma 3.3. Then Γ is a contraction map on $(\mathcal{G}_L, \|\cdot\|_{\mathcal{G}})$.*

Several lengthy estimates are needed in the proof of Lemma 3.5; we outline the steps here. Given $\Phi \in \mathcal{G}_L$, write $\Phi = T^* - \Psi$. Given $\eta \in \mathbb{R}$ and recalling $F(T^*, \eta) = 0$, one finds

$$\begin{aligned}\Gamma(\Phi)(\eta) &= \Phi(\beta) + F(\Phi(\beta), \beta)\\ &= (T^* - \Psi)(\beta) + \frac{K}{R}(B + C)\Psi(\beta) - \frac{KC}{R}\overline{\Psi(\beta)}\\ &= \left(1 - \frac{K(B+C)}{R}\right)(T^* - \Psi)(\beta) + \frac{KB}{R}T^*(\beta) + \frac{KC}{R}(T^*(\beta) - \overline{\Psi(\beta)}).\end{aligned}$$

Hence for all $\eta \in \mathbb{R}$,

$$\begin{aligned}\|\Gamma(\Phi)(\eta)\|_{\mathcal{B}} &\le \left(1 - \frac{KB}{R}\right)\|(T^* - \Psi)(\beta)\|_{\mathcal{B}} + \frac{KB}{R}\|T^*(\beta)\|_{\mathcal{B}}\\ &\le \left(1 - \frac{KB}{R}\right)L + \frac{KB}{R}L = L,\end{aligned}$$

using the fact Φ and T^* are each in $\mathcal{G}_L$. Hence $\|\Gamma(\Phi)\|_{\mathcal{G}} \le L$.

Showing $\mathrm{Lip}_{\mathcal{G}}(\Gamma(\Phi)) \le L$ and, for all $\eta \in \mathbb{R}$, $\mathrm{Lip}_{\mathbb{R}}(\Gamma(\Phi)(\eta)) \le L$, essentially follows from the estimates used above and properties of Lipschitz constants over sums of functions; details are in [41] . One concludes $\Gamma(\Phi) \in \mathcal{G}_L$.

To argue Γ is a contraction map, let $\Phi, \Psi \in \mathcal{G}_L$, $\eta \in \mathbb{R}$. Pick $x, z \in \mathbb{R}$ with

$$\eta = x + \varepsilon(\Phi(x)(x) - T_c) = z + \varepsilon(\Psi(z)(z) - T_c)$$

as in Lemma 3.3. By noting

$$\begin{aligned}|x - z| &= \varepsilon|\Phi(x)(x) - \Psi(z)(z)|\\ &\le \varepsilon(|\Phi(x)(x) - \Phi(x)(z)| + |\Phi(x)(z) - \Psi(x)(z)| + |\Psi(x)(z) - \Psi(z)(z)|),\end{aligned}$$

one can show $|x - z| \le \rho\|\Phi - \Psi\|_{\mathcal{G}}$, where ρ is as in Lemma 3.4. One then uses the observation $\|\Phi(x) - \Psi(z)\|_{\mathcal{B}} \le \|\Phi(x) - \Psi(x)\|_{\mathcal{B}} + \|\Psi(x) - \Psi(z)\|_{\mathcal{B}}$ to arrive at

$$\|\Phi(x) - \Psi(z)\|_{\mathcal{B}} \le (1 + \rho L)\|\Phi - \Psi\|_{\mathcal{G}},$$

after a few additional steps.

Now given $\eta \in \mathbb{R}$, one computes

$$\|\Gamma(\Phi)(\eta) - \Gamma(\Psi)(\eta)\|_{\mathcal{B}} = \|\Phi(x) + F(\Phi(x), x) - (\Psi(z) + F(\Psi(z), z))\|_{\mathcal{B}} =$$

$$\left\|\left(1 - \frac{K(B+C)}{R}\right)(\Phi(x) - \Psi(z)) + \frac{K}{R}Qs(y)(\alpha(y,z) - \alpha(y,x)) + \frac{KC}{R}(\overline{\Phi(x)} - \overline{\Psi(z)})\right\|_{\mathcal{B}}$$

$$\begin{aligned}&\le \left(1 - \frac{K(B+C)}{R}\right)\|\Phi(x) - \Psi(z)\|_{\mathcal{B}} + \frac{K}{R}QM|z - x| + \frac{KC}{R}\|\Phi(x) - \Psi(z)\|_{\mathcal{B}}\\ &\le \left(1 - \frac{KB}{R}\right)\|\Phi(x) - \Psi(z)\|_{\mathcal{B}} + \frac{K}{R}L|z - x|\\ &\le \left(1 - \frac{KB}{R}\right)(1 + \rho L)\|\Phi - \Psi\|_{\mathcal{G}} + \delta\rho\|\Phi - \Psi\|_{\mathcal{G}}\\ &= (B_0(1 + \rho L) + \delta\rho)\|\Phi - \Psi\|_{\mathcal{G}}.\end{aligned}$$

Note that $\mathrm{Lip}_{\mathcal{G}}(\alpha) = M$ was used above. Now recalling $B_0(1+\rho L)+\delta\rho < 1$ and noting η was arbitrary, we conclude Γ is a contraction map on the complete space $(\mathcal{G}_L, \|\cdot\|_{\mathcal{G}})$. □

The unique fixed point Φ^* of Γ satisfies $\Gamma(\Phi^*)(\eta) = \Phi^*(\eta)$ for every $\eta \in \mathbb{R}$, that is,

$$\Phi^*(\beta) + F(\Phi^*(\beta), \beta) = \Phi^*(\eta), \text{ where } \beta + \varepsilon(\Phi^*(\beta)(\beta) - T_c) = \eta.$$

To show $\mathcal{P}^*$ is invariant under the dynamic Budyko map m, let $(\Phi^*(\beta), \beta) \in \mathcal{P}^*$. As in the proof of Lemma 3.3, there exists $\hat{f}^* \in \mathcal{B}$ such that for all $\eta \in \mathbb{R}$,

$$\eta + \hat{f}^*(\eta) + \varepsilon(\Phi^*(\eta + \hat{f}^*(\eta))(\eta + \hat{f}^*(\eta)) - T_c) = \eta.$$

Pick η with $\beta = \eta + \hat{f}^*(\eta)$. We have

$$m(\Phi^*(\beta), \beta) = (\Phi^*(\beta) + F(\Phi^*(\beta), \beta), \eta) = (\Phi^*(\eta), \eta) \in \mathcal{P}^*.$$

We now show $\mathcal{P}^*$ is attracting under m in $\mathcal{B} \times \mathbb{R}$-space. Let

$$\tilde{\mathcal{B}} = \{f \in \mathcal{B} : \|f\|_{\mathcal{B}} \le L \text{ and } \mathrm{Lip}_{\mathbb{R}}(f) \le L\}.$$

Let $T_0 \in \tilde{\mathcal{B}}$, and set $\Phi_0 \in \mathcal{G}_L$ where, for all $\eta \in \mathbb{R}, \Phi_0(\eta) = T_0$. Let $\hat{f}_0$ and $\hat{f}^*$ denote the maps deduced in Lemma 3.3 corresponding to Φ_0 and Φ^*, respectively. Given $z \in \mathbb{R}$, pick $x, y \in \mathbb{R}$ such that $z = y + \hat{f}_0(y) = x + \hat{f}^*(x)$, that is,

$$y = z + \varepsilon(\Phi_0(z)(z) - T_c) \quad \text{and} \quad x = z + \varepsilon(\Phi^*(z)(z) - T_c).$$

Note

$$\|m((\Phi_0(z), z)) - m((\Phi^*(z), z))\|_{\mathcal{B}\times\mathbb{R}} = \|(\Gamma(\Phi_0)(y) - \Gamma(\Phi^*)(x), y - x)\|_{\mathcal{B}\times\mathbb{R}}.$$

We have $|y - x| = \varepsilon|\Phi_0(z)(z) - \Phi^*(z)(z)| \le \varepsilon\|\Phi_0(z) - \Phi^*(z)\|_{\mathcal{B}}$. Moreover, one can show

$$\begin{aligned}
\|\Gamma(\Phi_0)(y) - \Gamma(\Phi^*)(x)\|_{\mathcal{B}} &= \|\Phi_0(z) + F(\Phi_0(z), z) - (\Phi^*(z) + F(\Phi^*(z), z))\|_{\mathcal{B}} \\
&= \left\| \left(1 - \frac{K(B+C)}{R}\right)(\Phi_0(z) - \Phi^*(z)) + \frac{KC}{R}(\overline{\Phi_0(z)} - \overline{\Phi^*(z)}) \right\|_{\mathcal{B}} \\
&\le \left(1 - \frac{KB}{R}\right)\|\Phi_0(z) - \Phi^*(z)\|_{\mathcal{B}}.
\end{aligned}$$

Recalling ε and $1 - KB/R$ are each less than 1, we have

$$\|(\Gamma(\Phi_0)(y) - \Gamma(\Phi^*)(x), y - x)\|_{\mathcal{B}\times\mathbb{R}} \le \max\left\{\left(1 - \frac{KB}{R}\right)\|\Phi_0(z) - \Phi^*(z)\|_{\mathcal{B}},\ \varepsilon\|\Phi_0(z) - \Phi^*(z)\|_{\mathcal{B}}\right\}.$$

This proves $m^k(T_0, z)$ approaches $\mathcal{P}^*$ at an exponential rate and concludes the outline of the proof of Theorem 3.2. □

Remark 2. In the $\varepsilon = 0$ case the ice line position η remains fixed under recursion (12), with $m(\Phi(\eta), \eta) = (\Phi(\eta) + F(\Phi(\eta), \eta), \eta)$. In a manner directly analogous to the above, one can show

$$\|\Gamma(\Phi_0)(\eta) - \Gamma(T^*)(\eta)\|_{\mathcal{B}} \le \left(1 - \frac{KB}{R}\right)\|\Phi_0(\eta) - T^*(\eta)\|_{\mathcal{B}}.$$

Hence $\|m((\Phi_0(\eta), \eta)) - m((T^*(\eta), \eta))\|_{\mathcal{B}\times\mathbb{R}} \le (1 - \frac{KB}{R})\|(\Phi_0(\eta), \eta) - (T^*(\eta), \eta)\|_{\mathcal{B}\times\mathbb{R}}$, implying $\mathcal{T}^*$ is locally attracting under m when $\varepsilon = 0$ (see Figure 3).

Corollary 1. *The m-invariant manifold $\mathcal{P}^*$ is within $O(\varepsilon)$ of $\mathcal{T}^*$.*

The proof of this corollary requires one final estimate. Given $z \in \mathbb{R}$, pick $x \in \mathbb{R}$ with $z = x + \hat{f}^*(x)$. We have

$$\Phi^*(x) = \Phi^*(z) + F(\Phi^*(z), z) = \Phi^*(z) + F(\Phi^*(z) - T^*(z) + T^*(z), z).$$

Again using $F(T^*(z), z) = 0$, one finds via the reverse triangle inequality

$$\begin{aligned}\|\Phi^*(x) - \Phi^*(z)\|_{\mathcal{B}} &= \frac{K}{R}\|(B+C)(\Phi^*(z) - T^*(z)) - C(\overline{\Phi^*(z)} - \overline{T^*(z)})\|_{\mathcal{B}} \\ &\geq \frac{K}{R}\left[(B+C)\|\Phi^*(z) - T^*(z)\|_{\mathcal{B}} - C\|\Phi^*(z) - T^*(z)\|_{\mathcal{B}}\right] \\ &= \frac{KB}{R}\|\Phi^*(z) - T^*(z)\|_{\mathcal{B}}.\end{aligned}$$

Hence

$$\|\Phi^*(z) - T^*(z)\|_{\mathcal{B}} \leq \frac{R}{KB}\|\Phi^*(x) - \Phi^*(z)\|_{\mathcal{B}} \leq \frac{RL}{KB}|\hat{f}^*(x)|,$$

where the last inequality uses $z = x + \hat{f}^*(x)$ and $\Phi^* \in \mathcal{G}_L$. Recalling $\hat{f}^*(x) = \varepsilon(\Phi^*(z)(z) - T_c)$ and again using $\Phi^* \in \mathcal{G}_L$, we have

$$\|\Phi^*(z) - T^*(z)\|_{\mathcal{B}} \leq \frac{RL}{KB}\varepsilon|\Phi^*(z)(z) - T_c| \leq k_0\varepsilon,$$

where k_0 is independent of z. Hence for all $z \in \mathbb{R}$,

$$\|(\Phi^*(z), z) - (T^*(z), z)\|_{\mathcal{B}\times\mathbb{R}} = \max\{\|\Phi^*(z) - T^*(z)\|_{\mathcal{B}},\ z - z\} \leq k_0\varepsilon.$$

□

As a consequence of Theorem 3.2 and Corollary 1, the analysis of the infinite dimensional system (12) can be reduced to the study of the dynamics on the one dimensional m-invariant manifold $\mathcal{P}^*$. As $\|\Phi^*(z) - T^*(z)\|_{\mathcal{B}} \leq k_0\varepsilon$ for every $z \in \mathbb{R}$, with k_0 independent of z, we have $|\Phi^*(\eta)(\eta) - T^*(\eta, \eta))| \leq k_0\varepsilon$ for every ice line position $\eta \in \mathbb{R}$. As we'll see in the following section, the function

$$h : \mathbb{R} \to \mathbb{R},\ h(\eta) = T^*(\eta, \eta)$$

then determines the dynamics of the model.

3.3. **Dynamic Budyko model behavior.** Let $\alpha(y, \eta)$ be given by (8), and set $T_c = -10°\text{C}$ as in [38]. Recall that for $\varepsilon = 0$ and for any given η, there is a corresponding equilibrium temperature profile given by (13) with ice line η. Note that for $\varepsilon > 0$, fixed points (T, η) of the dynamic Budyko map m must satisfy $T(\eta) = T_c$, that is, the equilibrium temperature at the ice line must equal the critical temperature.

Motivated by Corollary 1 above, we plot $h(\eta) = T^*(\eta, \eta)$, the equilibrium temperature at the ice line when $\varepsilon = 0$, as a function of η in Figure 5. For typical parameters there are two equilibrium solutions for which the temperature at the ice line equals T_c. That is, there are two values $\eta_1 < \eta_2$ with $T^*(\eta_1, \eta_1) = -10°\text{C} = T^*(\eta_2, \eta_2)$. The ice line at η_1 corresponds to a large ice cap, while η_2 represents a small ice cap of the type we currently have on Earth.

The graph $\mathcal{P}^* = \{(\Phi^*(\eta), \eta) : \eta \in \mathbb{R}\}$ giving the attracting invariant manifold for the dynamic Budyko map m is within $O(\varepsilon)$ of $\mathcal{T}^* = \{(T^*(y, \eta), \eta) : \eta \in \mathbb{R}\}$ in the $\mathcal{B} \times \mathbb{R}$-norm. As shown above, we then have $\Phi^*(\eta)(\eta)$ is within $O(\varepsilon)$ of $T^*(\eta, \eta)$. This then implies the existence of $\hat{\eta}_1 < \hat{\eta}_2$, with $\hat{\eta}_i$ near η_i, and with $\Phi^*(\hat{\eta}_1)(\hat{\eta}_1) = T_c = \Phi^*(\hat{\eta}_2)(\hat{\eta}_2)$. Moreover, we also observe the following:

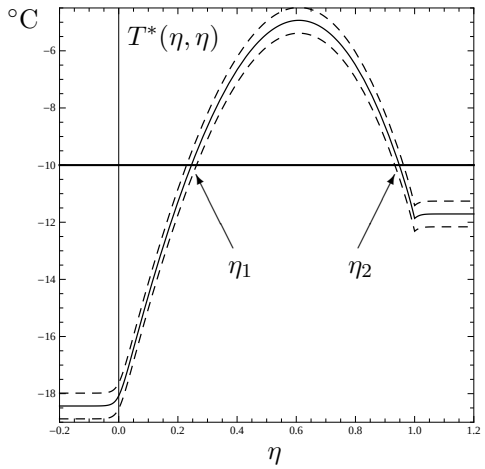

FIGURE 5. Solid curve: Temperature at the ice line η at equilibrium when $\varepsilon = 0$. Dashed curves: $T^*(\eta,\eta) \pm \varepsilon$. Parameters as in Figure 2.

(i) For $\eta > \hat{\eta}_2$, $\Phi^*(\eta)(\eta) < T_c$, implying ice will form and the ice line will descend toward $\hat{\eta}_2$.
(ii) For $\hat{\eta}_1 < \eta < \hat{\eta}_2$, $\Phi^*(\eta)(\eta) > T_c$, implying ice will melt and the ice line will move toward $\hat{\eta}_2$. We have that $(\Phi^*(\hat{\eta}_2), \hat{\eta}_2)$ is a stable fixed point of m.
(iii) For $\eta < \hat{\eta}_1$, $\Phi^*(\eta)(\eta) < T_c$, and again ice will form as the ice line moves equatorward. We have that $(\Phi^*(\hat{\eta}_1), \hat{\eta}_1)$ is an unstable fixed point of m.
(iv) As $\Phi^*(1)(1) < T_c$, the ice free Earth is an unstable state; the snowball Earth is a stable state in this model as $\Phi^*(0)(0) < T_c$.

We see that naturally incorporating a simple mechanism for movement of the ice line as the planet heats up or cools down provides for an improved, dynamically resolved energy balance climate model. The infinite dimensional system (14) reduces to the study of the dynamics on a one-dimensional invariant manifold, behavior which can be completely determined for $\alpha(y,\eta)$ as in (8). The emphasis of analyses of EBM had heretofore been placed on equilibrium solutions of the associated energy balance equation, with no recognition of the lack of any corresponding dynamical behavior.

The properties of the albedo function α used in the proof of Theorem 3.2 are that the map $\alpha : \mathbb{R} \to \mathcal{B}$, $\eta \mapsto \alpha(y,\eta)$ is an element of $\mathcal{G}$, with $\mathrm{Lip}_{\mathbb{R}}(\alpha(y,\eta)) \leq M$ for all $\eta \in \mathbb{R}$, and $\mathrm{Lip}_{\mathcal{G}}(\alpha) \leq M$. (This is the reason the constant M appears in the choice of L in (15).) It is natural then to ask whether the above approach can be extended to other energy balance models. We show this is the case in the following section, where an alternative albedo function leads to a scenario in which the model escapes the snowball Earth state, but with the ice line receding only to tropical latitudes.

4. The Jormungand global climate model.

4.1. **Neoproterozoic glaciations.** An abundance of geological and geochemical evidence indicates that ice sheets flowed into the ocean near the equator during two Neoproterozoic glacial periods, roughly 630 and 715 million years ago (Mya), respectively ([2], [4], [13], [16], [23]). Note that as the amount of snow and ice on the surface increases, the planetary albedo increases as well, and hence more insolation is reflected back into space. This positive *ice albedo feedback* causes the planet to cool further, so that the ice line continues to descend to lower latitudes. Given that glaciers advanced equatorward to such an extent during these glacial periods, some believe the Earth's ice albedo feedback ramped up to the point the planet became completely ice-covered ([14], [13], [17], for example). This is the so-called *snowball Earth* hypothesis.

There is also evidence, however, suggesting that photosynthetic eukaryotes, and perhaps various types of more biologically complex sponges, thrived both before and immediately after these glacial episodes ([1] and references therein). In a recent model introduced in [1], ice advances to 5-15° latitude, but a thin strip of ocean near the equator remains ice-free. This scenario is referred to as the *Jormungand* global climate state. In this fashion photosynthetic sea life could continue to exist, while glacial debris could flow into the ocean at low latitudes. The issue, however, is proposing a mechanism through which the planet is allowed to cool to the extent that glaciers exist in the tropics, yet not to the extent there is a runaway snowball Earth event.

4.2. **The Jormungand model.** Using atmospheric circulation considerations (the behavior of Hadley cells), as well as top-of-the-atmosphere albedo presumptions, an argument is made in [1] for net annual average evaporation in a latitude band centered at 15°–20° during the cold climate of the Neoproterozoic glaciations. This would imply sea ice forming in the tropics would not acquire a snow cover as there was insufficient precipitation relative to evaporation in this region. This leads to the incorporation of a bare sea ice albedo α_i, with $\alpha_w < \alpha_i < \alpha_s$, into the model. As bare sea ice absorbs more insolation than does snow covered sea ice, this furnishes a possible mechanism by which the advance of glaciers in the tropics might be halted prior to reaching the equator.

We introduce a Lipschitz continuous albedo function below which, when incorporated into Budyko's model and coupled with a dynamic ice line, serves to yield an attracting Jormungand global climate state. This albedo function is a continuous approximation to that used in [1], a work in which movement of the ice line was not considered. We note the ice line η will continue to represent the boundary between open ocean and (in this case, bare) sea ice.

Many of the parameter values used in the following are taken from [1], which in turn were chosen in part so that a Jormungand state could be found when running the Community Atmosphere Model, an atmospheric global system model at the National Center for Atmospheric Research. The main criterion needed is a significant difference between the bare sea ice albedo α_i and the snow covered ice albedo α_s.

We do note the solar constant Q was roughly 94% of its current value 600-700 Mya. Due to the vast amount of ice covering the planet during a Jormungand state, the draw-down of CO_2 from the atmosphere via silicate weathering [29] was also greatly reduced. As atmospheric CO_2 absorbs radiation in the infrared, this leads to a reduction in outgoing longwave radiation, modeled by a decrease in parameter

A from its current value. Finally, the ratio C/B is taken to be smaller during these glacial periods as meridional heat transport was less efficient, due in part to the extremely cold temperatures.

We assume no bare sea ice exists poleward of $y = 0.35$. We assume the latititudinal width of the bare sea ice is 0.35 when $\eta = 0$, and decreases linearly to zero when $\eta = 0.35$. Hence, the function

$$\delta(\eta) = \begin{cases} -\eta + 0.35, & \eta < 0.35 \\ 0, & \eta \geq 0.35 \end{cases}$$

represents the extent of any bare sea ice. Our albedo function is then

$$\alpha_J(y,\eta) = \frac{\alpha_s + \alpha_w}{2} + \frac{\alpha_i - \alpha_w}{2}\tanh(M(y-\eta)) + \frac{\alpha_s - \alpha_i}{2}\tanh(M(y-(\eta+\delta(\eta)))). \tag{17}$$

It is not difficult to show that each of $\mathrm{Lip}_{\mathbb{R}}(\alpha_J(\cdot,\eta))$ and $\mathrm{Lip}_{\mathcal{G}}(\alpha_J)$ is once again bounded above by M. Hence all estimates arising in the proof of Theorem 3.2 carry through unchanged if the albedo in (8) is replaced with (17) and the relationships in (15) hold. The dependence of the albedo α_J on the position of the ice line η is illustrated in Figure 6.

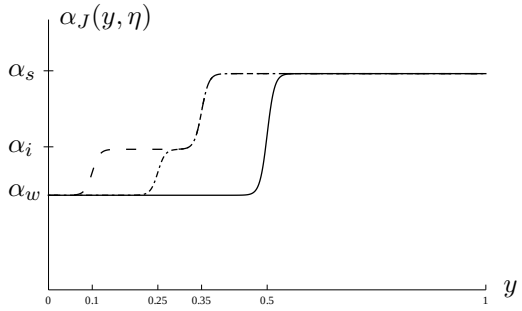

FIGURE 6. The albedo function given in (17). The extent of bare sea ice linearly shrinks to 0 as η increases through 0.35. Dashed: $\eta = 0.1$. Dash-Dot: $\eta = 0.25$. Solid: $\eta = 0.5$.

4.3. **Invariant manifold in the coupled Jormungand–ice line model.** We consider (4) with albedo function α_J given by (17). As in section 2.2, equilibrium solutions are given by

$$T_J^*(y,\eta) = \frac{1}{B+C}\left(Qs(y)(1-\alpha_J(y,\eta)) + Q\frac{C}{B}(1-\overline{\alpha}_J(\eta)) - A\left(1+\frac{C}{B}\right)\right),$$

with a revised

$$\overline{\alpha}_J(\eta) = \int_0^1 s(y)\alpha_J(y,\eta)dy.$$

We plot several such solutions in Figure 7, and once again note the equilibrium temperature profile depends explicitly on η. Moreover, given any $\eta \in [0,1]$ there is an equilibrium solution of (4) having an ice line at η. The equilibrium solutions embedded in $\mathbb{R}$ are correspondingly given by (13) with $\alpha(y,\eta)$ replaced by $\alpha_J(y,\eta)$.

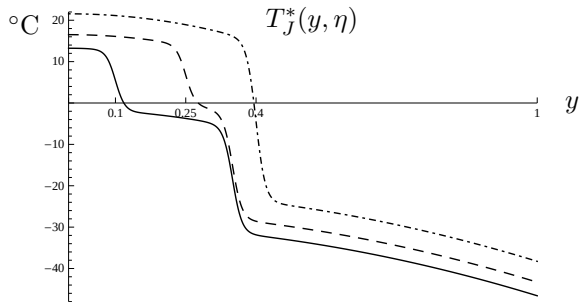

FIGURE 7. Equilibrium solutions of (4) with albedo function (17). Solid: $\eta = 0.1$. Dashed: $\eta = 0.25$. Dash-Dot: $\eta = 0.4$. Parameters: $Q = 321, A = 167, B = 1.5, C = 2.25, M = 50, \alpha_w = 0.32, \alpha_i = 0.46, \alpha_s = 0.72$.

To impart a dynamics perspective, the Jormungand model may be coupled with an equation for the evolution of η, as in Section 3. We consider the dynamic Budyko map for the Jormungand model

$$m_J : \mathcal{B} \times \mathbb{R} \to \mathcal{B} \times \mathbb{R},\ m_J(T(y), \eta)) = (T(y) + F(T(y), \eta),\ \eta + G(T(y), \eta)), \quad (18)$$

with $F(T, \eta)$ as in (11) but with $\alpha(y, \eta)$ replaced by $\alpha_J(y, \eta)$, and $G(T, \eta)$ as in (12).

Our albedo function $\alpha_J(y, \eta)$ has been constructed to satisfy the criteria of Theorem 3.2. For the $\varepsilon = 0$ case,

$$\mathcal{T}_J^* = \{(T_J^*(y, \eta), \eta) : \eta \in \mathbb{R}\}$$

is an attracting m_J-invariant manifold comprised of fixed points. For $\varepsilon > 0$ and sufficiently small there exists a locally attracting invariant manifold

$$\mathcal{P}_J^* = \{(\Phi_J^*(\eta), \eta) : \eta \in \mathbb{R}\},$$

which is within $O(\varepsilon)$ of $\mathcal{T}_J^*$, as in Section 3. The study of the dynamics of mapping m_J for the Jormungand–ice line model is reduced to determining the model behavior on $\mathcal{P}_J^*$.

Due to the fact there are smaller seasonal variations in temperature near the equator, ice which formed near the low-latitude ice line was less likely to melt over the course of a year if the ice line temperature was near freezing. Thus in the Jormungand model the critical temperature is taken to be $T_c = 0°\text{C}$ [1]. Given the albedo function $\alpha_J(y, \eta)$, one can rigorously show the existence of three η-values for which $T_J^*(\eta, \eta) = 0°\text{C}$ for our choice of parameters.

In Figure 8 we plot the equilibrium temperature at the ice line $h(\eta) = T_J^*(\eta, \eta)$. Recalling the attracting invariant manifold $\{(\Phi_J^*(\eta), \eta) : \eta \in \mathbb{R}\}$ is within $O(\varepsilon)$ of $\{(T_J^*(y, \eta), \eta) : \eta \in \mathbb{R}\}$ in the $\mathcal{B} \times \mathbb{R}$-norm, we again have that $\Phi_J^*(\eta)(\eta)$ is within $O(\varepsilon)$ of $T_J^*(\eta, \eta)$. We conclude there exist $\hat{\eta}_1 < \hat{\eta}_2 < \hat{\eta}_3$ with $\Phi_J^*(\hat{\eta}_i)(\hat{\eta}_i) = 0°\text{C}$, and hence mapping (18) has three fixed points on $\mathcal{P}_J^*$. Via an analysis similar to that provided in Section 3.3, we see that $(\Phi_J^*(\hat{\eta}_1), \hat{\eta}_1)$ and $(\Phi_J^*(\hat{\eta}_3), \hat{\eta}_3)$ are each attracting, while $(\Phi_J^*(\hat{\eta}_2), \hat{\eta}_2)$ is unstable. We thus have a stable equilibrium solution for the coupled Jormungand model for which the ice line lies in lower latitudes.

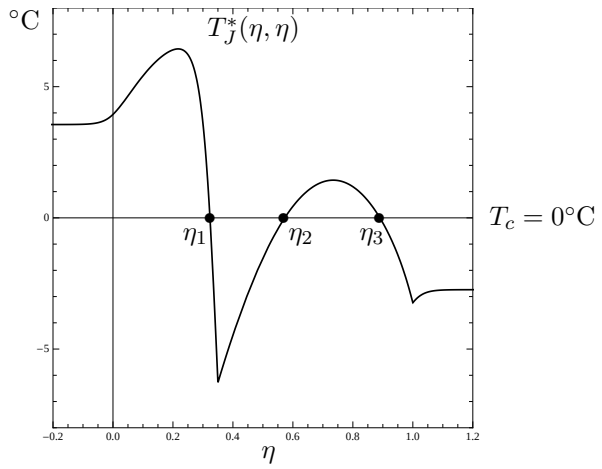

FIGURE 8. Temperature at equilibrium at the ice line with albedo function (17) when $\varepsilon = 0$. Parameters as in Figure 7.

We also note that, as for the dynamic Budyko map m with albedo function (8), the ice free state is unstable. The snowball Earth state, however, is unstable in the Jormungand model as $\Phi_J^*(0)(0) > 0°\text{C}$. This is a consequence of the lower albedo α_i of the bare sea ice forming near the equator, relative to α_s.

4.4. **Bifurcations.** We investigate the behavior of m_J-orbits on the attracting invariant manifold $\mathcal{P}_J^*$ as parameters are varied. In this section we focus on the parameter A, though other parameters may be adjusted as well. Recall that A is the constant term in the approximation used for the outgoing longwave radiation in the model formulation. As the concentration of greenhouse gasses such as CO_2 increases, more longwave radiation is absorbed by the atmosphere, leading to a decrease in the parameter A. Similarly, as the concentration of greenhouse gasses decreases, more longwave radiation escapes to space, leading to an increase in the parameter A. In this fashion one can consider A as serving as a proxy for greenhouse gas concentrations, though the rise and fall of the former is opposite that of the latter.

Many authors have previously discussed bifurcations in EBM ([1], [9], [10], [31], [38], and references therein). Each of these treatments, however, is lacking in that none considers movement of the ice line with changes in temperature. (Indeed, there is a common assumption the climate system is always in equilibrium.) Bifurcations of solutions of (1) as a parameter varies are presented in these studies with no consideration of the dynamical nature of the equilibrium point in question. The introduction of the ice line equation in (10), and the analysis of the coupled (T, η)-system initiated in [41], places the study of bifurcations in EBM on firm mathematical footing.

We plot the parameter A versus the position of the ice line in Figure 9. More specifically, given η we compute the corresponding A-value for which $T_J^*(\eta, \eta) = 0 = T_c$. The horizontal line $A = A_2$ in Figure 9 indicates the A-value used in the plot

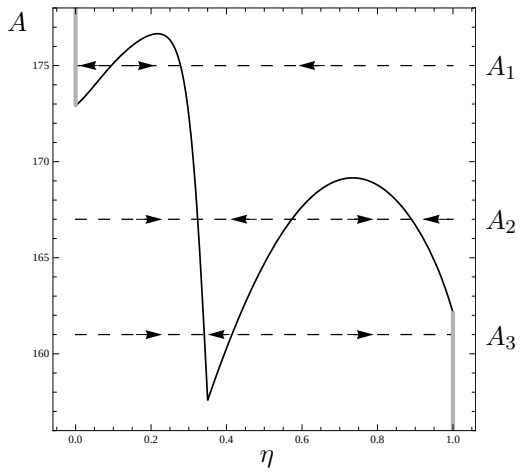

FIGURE 9. Bifurcation plot in the (η, A)-plane. The solid black curve gives (η, A) pairs for which $T^*(\eta, \eta) = 0°\text{C}$. The vertical gray lines correspond to an ice free planet (right) and snowball Earth (left). Parameters as in Figure 8.

shown in Figure 8, with the arrows indicating the movement of the ice line for that A-value. Hence the intersection points $\eta_1 < \eta_2 < \eta_3$ of $A = A_2$ with the (η, A)-curve correspond to the three fixed points lying on $\mathcal{P}_J^*$ discussed in the previous section.

We note there are several bifurcations as A decreases from 178 to 156 W/m^2. Horizontal line $A = A_1$ in Figure 9 corresponds to the scenario in which there is a stable large ice cap, and an unstable equilibrium solution with ice line very near the equator. The vertical gray line to the left in Figure 9 corresponds to the snowball Earth state, which is stable for sufficiently high A-values.

For lower values of A, such as that corresponding to line $A = A_3$ in Figure 9, there exist a large stable ice cap, a slightly smaller unstable ice cap at equilibrium, and a stable ice free Earth (represented by the vertical line to the right in the figure).

Given the parameter values associated with the great Neoproterozoic glaciations, it is the behavior of the model for A-values nearer A_2 in Figure 9 which are of greatest interest in this section. Note the fixed point corresponding to the large ice cap is attracting for an interval of parameter values centered at $A = 167$. As A increases through roughly 169 W/m^2, however, the stable small ice cap solution disappears, and the system evolves toward an equilibrium solution with ice line at roughly $\sin^{-1}(0.3)$. In the Jormungand model, the lower albedo of the bare sea ice near the equator, relative to the albedo of the snow covered sea ice, serves to tamp down the positive ice albedo feedback sufficiently so as to avoid a snowball Earth.

5. **Incorporating land into the model.** The models analyzed to this point assume the surface of the planet is comprised entirely of water and ice. In terms of albedo, two variations of ice—bare and snow covered—are considered. Though the

surface of the Earth is three-fourths water, so that a water planet may serve as a viable approximation, it is nevertheless desirable to include land mass, and its distribution, in the model.

The position and topology of continental land masses on Earth have changed significantly over geologic time scales. During the Neoproterozoic Era, for example, most of the land was clustered in lower latitudes about the equator [14]. Roughly 300 Mya, there was but one large, connected continental land mass [20].

In this section we incorporate land into the dynamic Budyko model to further illustrate the utility of Theorem 3.2. We assume a symmetry in both temperature and land placement across the equator, so that once again $y \in [0, 1]$. As in [19], we consider a *band* or *annulus* of land extending from latitude η_1 northward to latitude η_2, with $0 \leq \eta_1 < \eta_2 \leq 1$. There is then a symmetrically positioned band in the southern hemisphere. Striving for simplicity, we do not adjust the heat capacity of the Earth's surface so that it varies with latitude, as in [19].

As a first example we assume there is no ice on the planet. Such warmer climates prevailed many times in Earth's history, with but one example furnished by the period leading up to and during the Palaeocene-Eocene Thermal Maximum [34]. We choose an albedo function such as that plotted in Figure 10, using an albedo value α_ℓ for land which is larger than α_w. We also ensure the albedo function has appropriate bounds on its Lipschitz constants, enabling us to use results in Section 3. The function

$$\alpha(y, \eta) = \alpha_w + \frac{\alpha_\ell - \alpha_w}{2} \tanh(M(y - \eta_1)) - \frac{\alpha_\ell - \alpha_w}{2} \tanh(M(y - \eta_2)) \tag{19}$$

is an example of such an albedo function.

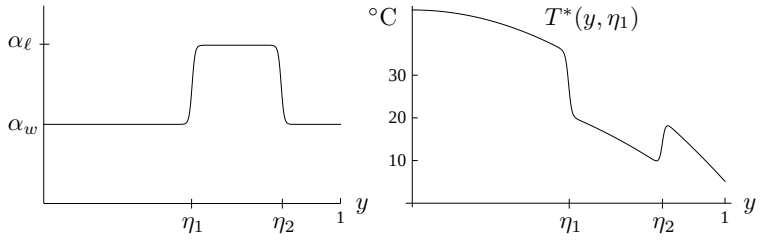

FIGURE 10. *Left*: Albedo function for an ice free Earth with a band of land on the annulus $\eta_1 \leq y \leq \eta_2$. *Right*: The corresponding attracting equilibrium temperature profile.

Note the lower bound η_1 of the land annulus can be viewed as a non-dynamic ice line, that is, we can construct a system analogous to (12), albeit with $\varepsilon = 0$ and η_1 playing the role of the (fixed) ice line η. We conclude that, given a prescribed value of η_1, there exists a locally attracting temperature profile $T^*(y, \eta_1)$ as in Figure 10. The qualitative behavior of the surface temperature over time is independent of the placement of the land mass. We see the equilibrium temperature over land is lower

than that over the ocean due to the fact land reflects insolation more effectively than does water.

For a second and more dynamic example we return to the Neoproterozoic Era, now placing the annulus of land about the equator [15]. We thus assume land extends from the equator northward to $y = 0.35$. As before, we let η represent the boundary between sea ice and open ocean water. Assuming a paucity of precipitation relative to evaporation in lower latitudes as in [1], we further assume glaciers do not form easily near sea level on land.

We thus have three distinct albedo values $\alpha_w < \alpha_\ell < \alpha_s$, where α_ℓ represents the albedo of land. For the associated albedo function we choose

$$\alpha(y,\eta) = \begin{cases} \frac{\alpha_s+\alpha_\ell}{2} + \frac{\alpha_s-\alpha_\ell}{2}\tanh(M(y-.35)), & \eta < 0.35 \\ \frac{\alpha_s+\alpha_\ell}{2} - \frac{\alpha_\ell-\alpha_w}{2}\tanh(M(y-.35)) + \frac{\alpha_s-\alpha_w}{2}\tanh(M(y-\eta)), & \eta \geq 0.35. \end{cases} \tag{20}$$

The surface albedo as a function of the ice line is illustrated in Figure 11. Note that if $\zeta < \eta < 0.35$, $\alpha(y,\zeta) = \alpha(y,\eta)$, which corresponds in the model to the restriction of the ice line from moving significantly over land. We also note M serves as an upper bound for both Lipschitz constants $\mathrm{Lip}_{\mathbb{R}}(\alpha(\cdot,\eta))$ and $\mathrm{Lip}_{\mathcal{G}}(\alpha)$ for $\alpha(y,\eta)$ as in (20).

While recognizing the geophysical process modeled above lacks a mechanism by which η might lie near the equator, given the definition of the albedo function (20) for $\eta \in [0, 0.35)$, we can nonetheless invoke Theorem 3.2 in a meaningful way. Sketched in Figure 12 is the equilibrium temperature at the ice line $T^*(\eta,\eta)$ when $\varepsilon = 0$, with albedo function (20). We see this model admits two distinct possibilities for stable asymptotic behavior. The attracting fixed point for the dynamic Budyko map corresponding to η_3 in Figure 12 represents an ice cap positioned at roughly 46° N. The attracting fixed point corresponding to η_1 in Figure 12, just below $\eta = 0.35$, represents a planet with no open water, albeit one with a lack of ice cover over the band of land.

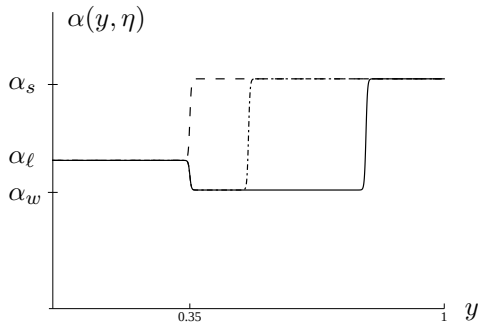

FIGURE 11. The albedo function given in (20). Dashed: $\eta = 0.2$. Dash-Dot: $\eta = 0.5$. Solid: $\eta = 0.8$.

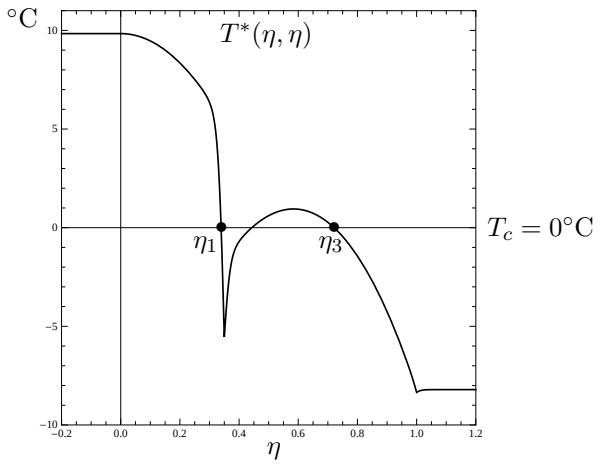

FIGURE 12. Temperature at equilibrium at the ice line with albedo function (20) when $\varepsilon = 0$. Parameters: $Q = 321, A = 172, B = 1.5, C = 2.25, M = 50, \alpha_w = 0.32, \alpha_\ell = 0.4, \alpha_s = 0.62$.

Further development of the model might include the presence of glaciers in mountainous regions on the annulus of land [25]. The role of the ice line η would remain the same. Due to the existence of mountain glaciers, however, we now consider a second ice line, denoted by ζ, representing the boundary between ice covered and bare land. This then necessitates a second ice line equation for the evolution of ζ, as well as a corresponding extension of Theorem 3.2. Noting that EBM provide only broad perspectives on a few, large-scale factors in climate dynamics, this model would nonetheless incorporate the role of geography into the ice-albedo feedback process in a more realistic fashion, while remaining accessible to mathematical analysis. Such an analysis would naturally extend results presented in this paper.

6. **Conclusion.** The study of large scale planetary and atmospheric climate processes provides for a host of interesting mathematical modeling problems. Latitude-dependent energy balance models, such as those introduced by Budyko and Sellers in 1969, have been extensively studied. In all previous works, however, no attention was given to the dynamical nature of equilibrium solutions of the governing equation. Analyses of bifurcations of equilibrium points were presented in various articles without first determining if the equilibrium solutions were stable or unstable. Fundamental questions, such as what happens to the evolution of the surface temperature for fixed parameter values if the system isn't started at the equilibrium temperature profile, had yet to be addressed.

In recent work Budyko's model was coupled with a dynamic ice line [41]: as the planet cools off (respectively, heats up), the ice line moves equatorward (respectively, poleward). Given certain conditions imposed on the smoothness of the albedo and temperature distribution functions, as well as on model parameters, Widiasih proved

the existence of a one-dimensional attracting invariant manifold in the temperature–ice line state space, leading to a complete understanding of model behavior.

In this work the mathematical approach to the study of EBM is continued and expanded upon, firmly placing such models in a dynamical systems context. Theorem 3.2 can be applied to the coupled Budyko–ice line model with a variety of albedo functions, such as that appropriate for the Jormungand global climate model, as well as others which take into consideration the presence of land. Rich possibilities exist for further progress in the mathematical analysis of energy balance models arising in the study of climate.

Acknowledgments. J.W. thanks the School of Mathematics at the University of Minnesota for its support during a recent sabbatical visit, during which this work began. E.W. was supported in part by a grant to the University of Arizona from HHMI (52006942). We thank Richard McGehee and collaborators at the Mathematics of Climate Research Network for their support, and we thank the referees for insightful comments on an earlier draft of this paper.

REFERENCES

[1] D. Abbot, A. Viogt and D. Koll, The Jormungand global climate state and implications for Neoproterozoic glaciations, *J. Geophys. Res.*, **116** (2011).
[2] H. Bao, J. Lyons and C. Zhou, Triple oxygen isotope evidence for elevated CO_2 levels after a Neoproterozoic glaciation, *Nature*, **453** (2008), 504–506.
[3] P. Bates, K. Lu and C. Zeng, Existence and persistence of invariant manifolds for semiflows in Banach space, *Memoirs of the American Mathematical Society*, Providence, RI, **135** (1998).
[4] B. Bodiselitsch, C. Koeberl, S. Master and W. Reimold, Estimating duration and intensity of Neoproterozoic snowball glaciations from Ir anomalies, *Science*, **308** (2005), 239–242.
[5] H. Broer, C. Simó and R. Vitolo, Bifurcations and strange attractors in the Lorenz-84 climate model with seasonal forcing, *Nonlinearity*, **15** (2002), 1205–1267.
[6] H. Broer and R. Vitolo, Dynamical systems modeling of low-frequency variability in low-order atmospheric models, *Disc. Cont. Dyn. Syst. B*, **10** (2008), 401–419.
[7] H. Broer, H. Dijkstra, C. Simó, A. Sterk and R. Vitolo, The dynamics of a low-order model for the Atlantic multidecadal oscillation, *Disc. Cont. Dyn. Syst. B*, **16** (2011), 73–102.
[8] M. I. Budyko, The effect of solar radiation variation on the climate of the Earth, *Tellus*, **5** (1969), 611–619.
[9] R. Cahalan and G. North, A stability theorem for energy-balance climate modes, *J. Atmos. Sci.*, **36** (1979), 1178–1188.
[10] P. Chylek and J. A. Coakley, Analytical analysis of a Budyko-type climate model, *J. Atmos. Sci.*, **32** (1975), 675–679.
[11] M. Claussen et al, *Earth system models of intermediate complexity: Closing the gap in the spectrum of climate models*, *Climate Dynamics*, **18** (2002), 579–586.
[12] C. Graves, W-H. Lee and G. North, New parameterizations and sensitivities for simple climate models, *J. Geophys. Res.*, **198** (1993), 5025–5036.
[13] P. Hoffman, A. Kaufman, G. Halverson and D. Schrag, A Neoproterozoic snowball Earth, *Science*, **281** (1998), 1342–1346.
[14] P. Hoffman and D. Schrag Snowball Earth, *Sci. Amer.*, **282** (2000), 68–75.
[15] P. Hoffman and D. Schrag, The snowball Earth hypothesis: Testing the limits of global change, *Terra Nova*, **14** (2002), 129–155.
[16] R. Kerr, Snowball Earth has melted back to a profound wintry mix, *Science*, **327** (2010), 1186.
[17] J. Kirschivink, Late Proterozoic low-latitude global glaciation: the snowball Earth, in *The Proterozoic Biosphere: A Multidisciplinary Study* (eds. J. Schopf and C. Klein), Cambridge University Press, 1992, section 2.3.
[18] W. Langford and G. Lewis, Poleward expansion of Hadley cells, *Can. Appl. Math. Quart.*, **17** (2009), 105–119.
[19] R. Q. Lin and G. North, A study of abrupt climate change in a simple nonlinear climate model, *Climate Dynamics*, **4** (1990), 253–261.

[20] R. A. Livermore, A. G. Smith and F. J. Vine, Late Palaeozoic to early mesozoic evolution of Pangaea, *Nature*, **322** (1986), 162–165.
[21] E. Lorenz, Irregularity: A fundamental property of the atmosphere, *Tellus*, **36A** (1984), 98–110.
[22] L. Maas, A simple model for the three-dimensional, thermally and wind-driven ocean circulation, *Tellus*, **46A** (1994), 671–680.
[23] F. Macdonald, M. Schmitz, J. Crowley, C. Root, D. Jones, A. Maloof, J. Strauss, P. Cohen, D. Johnston and D. Schrag, Calibrating the cryogenian, *Science*, **327** (2010), 1241–1243.
[24] H. Marshall, J. Walker and W. Kuhn, Long-term climate change and the geochemical cycle of carbon, *J. Geophys. Res.*, **93** (1988), 791–801.
[25] R. McGehee, personal communication.
[26] R. McGehee and C. Lehman, A paleoclimate model of ice-albedo feedback forced by variations in Earth's orbit, *SIAM J. Appl. Dyn. Syst.*, **11** (2012), 684–707.
[27] R. McGehee and E. Widiasih, A finite dimensional version of a dynamic ice-albedo feedback model, preprint.
[28] G. North, Theory of energy-balance climate models, *J. Atmos. Sci.*, **32** (1975), 2033–2043.
[29] R. Pierrehumbert, *Principles of Planetary Climate*, Cambridge University Press, New York, 2010.
[30] C. Robinson, *Dynamical Systems: Stability, Symbolic Dynamics, and Chaos*, CRC Press, Boca Raton, FL, 1995.
[31] G. Roe and M. Baker, Note on a catastrophe: A feedback analysis of snowball Earth, *J. of Climate*, **23** (2010), 4694–4703.
[32] P. Roebber, Climate variability in a low-order coupled atmosphere-ocean model, *Tellus*, **47A** (1995), 473–494.
[33] C. Sagan and G. Mullen, Earth and Mars: Evolution of atmospheres and surface temperatures, *Science*, **177** (1972), 52–56.
[34] R. Secord, P. Gingerich, K. Lohmann and K. MacLeod, Continental warming preceding the Palaeocene-Eocene thermal maximum, *Nature*, **467** (2010), 955–959.
[35] W. Sellers, A global climatic model based on the energy balance of the Earth-Atmosphere system, *J. Appl. Meteor.*, **8** (1969), 392–400.
[36] A. Shil'nikov, G. Nicolis and C. Nicolis, Bifurcation and predictability analysis of a low-order atmospheric circulation model, *Int. J. Bif. Chaos*, **5** (1995), 1701–1711.
[37] H. E. de Swart, Low-order spectral models of the atmospheric circulation: A survey, *Acta Appl. Math.*, **11** (1988), 49–96.
[38] K. K. Tung, *Topics in Mathematical Modeling*, Princeton University Press, Princeton, New Jersey, 2007.
[39] L. van Veen, Overturning and wind driven circulation in a low-order ocean-atmosphere model, *Dynam. Atmos. Ocean*, **37** (2003), 197–221.
[40] L. van Veen, Baroclinic flow and the Lorenz-84 model, *Int. J. Bif. Chaos*, **13** (2003), 2117–2139.
[41] E. Widiasih, Instability of the ice free earth: Dynamics of a discrete time energy balance model, preprint `arXiv:1105.4918`.

Received May 2012; 1st revision May 2012, 2nd revision August 2013.

E-mail address: jawalsh@oberlin.edu
E-mail address: widiasih@hawaii.edu